Eur. Phys. J. Special Topics **146**, 261–277 (2007)

DOI: 10.1140/epjst/e2007-00185-8

THE EUROPEAN PHYSICAL JOURNAL SPECIAL TOPICS

Numerical simulations of binary fluid convection in large aspect ratio annular containers

A. Alonso[a], O. Batiste, and I. Mercader

Departament de Física Aplicada, Universitat Politècnica de Catalunya, Mòdul B4, 08034 Barcelona, Spain

Abstract. The patterns arising in large aspect ratio annular containers heated from below are analyzed for water-ethanol mixtures with negative Soret coupling. The subcritical Hopf bifurcation at the onset of convection leads to a very rich dynamics. Using high resolution numerical tools based on spectral methods to solve the hydrodynamic equations we obtain and review the properties of the different regimes arising in early stages of convection: spatially extended stationary and travelling wave convective roll structures, dispersive chaotic states, and several types of localized convection. The dynamics triggered by the Eckhaus–Benjamin–Feir instability is presented for a mixture with a moderate negative value of the separation ratio.

1 Introduction

Thermal convection in binary fluid mixtures has attracted much research activity in the past and has become a paradigmatic experimental system for the study of nonlinear wave phenomena and pattern formation [1]. In comparison to the pure fluid case, where complex dynamics near the onset of convection is only observed near strong resonances (for an example, the dynamics near the 1:2 resonance is analyzed in [2] in a Bénard–Marangoni cylinder and in [3] in a non-Boussinesq Rayleigh–Bénard configuration), the dynamics near the threshold can be much more complicated in binary mixtures due to the extra degree of freedom associated with the concentration field. In a pure fluid a temperature gradient produces a density gradient and the fluid becomes potentially unstable in the presence of gravity. In a binary mixture, the temperature gradient also produces a flux of mass (Soret effect). The density gradient is thus modified by the concentration gradient induced by the Soret effect. The nondimensional parameter that quantifies the influence of this effect on the convective buoyancy force is the separation ratio S. When $S > 0$ the denser component tends to move towards the colder region. The threshold of instability is dramatically lowered, the critical wavelength of the pattern tends to infinity, but the arising convective pattern remains stationary [4]. If $S < 0$ the denser component migrates towards the hotter region, with the Soret diffusion having a stabilizing effect on the fluid layer. In this case, provided S is negative enough, the first instability of the conduction state is already oscillatory. This fact makes the system very interesting from the point of view of dynamical systems, because it leads to a rich dynamical behaviour near the onset of convection.

Experiments on binary mixtures are frequently made using different types of solutions of ethanol in water, for which the value of the separation ratio can range typically from -0.5 to $+0.5$, although other types of solutions, such as mixtures of ^{3}He–^{4}He, have also been used. When the specific weights of the two components are quite distinct, such in the case of ferrofluids (dispersions of magnetite in water or oil), the binary mixture is known to exhibit a large

[a] e-mail: arantxa@fa.upc.edu

value of the separation ratio ($|S| \sim 10$ or even larger). In our work, we will focus on binary mixtures with negative values of the separation ratio in the range $|S| \leq 1$.

In order to achieve translation invariant systems that can support uniform travelling waves, experiments are usually performed on long, narrow annular cells. For mixtures with negative values of the separation ratio, different behaviours have been observed depending on the actual strength of S. In the case of the experiment reported in [5] a $S = -0.257$ water-ethanol mixture is used. A final state consisting of large amplitude nearly 2D uniform travelling waves is observed when the threshold of stability of the conduction state is crossed. This TW branch is found to be stable until a saddle-node bifurcation is reached by decreasing the Rayleigh number. If the Rayleigh number is increased above a certain critical value, travelling waves disappear and give rise to stationary states, which are often named in literature steady overturning convection states (SOC states) [6]. In contrast, for mixtures with a separation ratio value closer to zero, such as the $S = -0.021$ binary mixture used in experiment [7], uniform travelling waves are never observed, despite numerical computations confirming their existence. These completely different behaviours may be attributed to the different stability properties of the travelling wave solutions in extended domains, due to Eckhaus–Benjamin–Feir instabilities (instabilities that modify the periodicity of the basic solution in the TW branch). At least two experimental papers, using $S = -0.26$ and $S = -0.127$ mixtures, have been devoted to the determination of the Eckhaus stability boundaries of travelling waves in binary fluid convection [8,9].

Apart from uniform travelling wave convection and steady convection, experiments show that binary fluid mixtures with negative values of S exhibit a tendency to form spatially confined patterns. Among these types of patterns, localized travelling waves (LTWs) arise very frequently, as reported in several experiments [10–14]. In such persistent patterns, TWs are observed in isolated regions surrounded by motionless fluid. Slow and fast LTW convection can be distinguished, as well as very narrow confined states and wider structures. Pulses of TW convection (very narrow localized states) are indeed ubiquitous in binary convection, and are very difficult to avoid on this system. For this reason, the extensive experimental study dealing with the existence and stability properties of TW pulses, the interaction between them, and the dynamics of the TW fronts has been completed with numerical and analytical work on complex Ginzburg Landau models, and with the numerical integration of the full Navier-Stokes equations [6,15–18].

The ubiquity of LTWs in a large number of studies on binary Rayleigh–Bénard convection contrasts with the scarce references to localized stationary states. Very recent numerical simulations have shown that spatially localized steady states such as those present in magnetoconvection [19] can also arise in the context of binary mixture convection. Following [19], such states have been named *convectons* to distinguish them from other localized states, and consist of regions of steady large-amplitude convection coexisting with quiescent fluid. Although initially convectons were obtained by direct numerical simulation (DNS) of the full hydrodynamic equations in ^{3}He–^{4}He mixtures (mixtures with a strong negative value of the Soret coupling) [20,21], subsequent simulations [22] have revealed that they can also be present in water-ethanol mixtures, which are much more convenient for experimental studies. For the time being, convectons have only been reported in one experiment [23], even though surrounding waves were also present in that case, so the pattern was not stationary.

In addition to the previous patterns, a series of experiments on mixtures with separation ratio of around $S = -0.02$ [7,23] show that, near the onset of the primary instability, the weakly nonlinear oscillatory convection can be in the form of small-amplitude states and can exhibit dispersive chaos, which is a dynamical state characterized by an erratic growth and decay of the convection amplitude. These small-amplitude waves consist of the repetitive formation and sudden collapse of spatially localized pulses that lead to erratic dynamics with no stable saturated state. These states are never observed for mixtures with a larger value of $|S|$. Dispersive chaotic states obtained by DNS of the full convection equations have been obtained for the first time in a very recent work [24].

The purpose of our work is to study numerically by DNS of the hydrodynamic equations the patterns arising in binary convection in large aspect ratio annular containers and to analyze

the complex dynamics observed in experiments in early stages of convection. To that aim, we have developed several accurate numerical tools based on spectral methods that enable us to compute the arising nonlinear patterns. The main difficulty in modelling this system numerically is the large size of the annular containers used in experiments. Since all the patterns reported in experiments are essentially two-dimensional (2D), the first simplification assumed in the available numerical works is to neglect variations along the spanwise direction. Most of the results discussed in this paper correspond to 2D simulations.

Computations can also be significantly reduced in the case of spatially extended stationary and travelling wave convective roll structures. For such solutions, only a pair of rolls needs to be considered, so the size of the domain can be reduced to a single wavelength. In this way, in a very extensive and thorough work, Barten et al. [25] were able to study in detail the branches of travelling waves (TW) and steady states (SOC) for different values of the separation ratio. These authors obtained the bifurcation diagrams of the uniform TW and SOC states, located the transition between them, and analyzed the properties of the different fields, paying special attention to the structure of the concentration field.

However, this type of study cannot describe the highly spatially non-uniform states observed during the dispersive chaos regime, the travelling and stationary localized states or the dynamics arising from Eckhaus–Benjamin–Feir instabilities. The numerical works devoted to obtaining non-uniform solutions are less abundant.

On one hand, Barten, Lücke et al. (see, for instance, [26]) developed a finite difference code to model binary convection in an extended container. Among other works, they analyzed the dynamics of localized travelling waves and of travelling wave fronts [6,16–18]. Additionally, Huke et al. [27] analyzed the stability of steady rolls and square convection for positive separation ratio mixtures, including in their analysis the Eckhaus instability. In Büchel et al. [28] transitions between different wavenumber travelling wave patterns were observed for negative separation ratios and the dynamics was explained as a manifestation of Eckhaus instabilities. Nevertheless, narrow rectangular containers were considered in their simulations, so the pattern selection dynamics was influenced by the presence of lateral boundaries.

On the other hand, spectral methods were used by Mercader, Batiste et al. to study the dynamics in large aspect ratio rectangular containers [29] and to compute the Eckhaus instability of travelling waves in annular cells [30]. These types of techniques have also been used in very recent works to obtain for the first time in binary convection both stable and unstable stationary localized states [20–22], and to obtain and analyze the very rich spatiotemporal dynamics observed during the dispersive–chaotic regime for mixtures with a weak negative Soret coupling [24]. The question of the influence of the transverse walls on the onset of convection was addressed in [31], where a three dimensional linear stability analysis of the basic conductive state was carried out.

In this paper, we review the main properties of the different patterns observed in binary convection not far from the onset of convection. Most of these patterns have been obtained numerically in very recent works [22,24,30,31]. In addition, we present new simulations describing the dynamics triggered by the Eckhaus–Benjamin–Feir instability for a mixture with a moderate negative value of the separation ratio. All the states discussed in this paper arise in large annular containers whose aspect ratio lies between 60 and 84, and for several types of water-ethanol mixtures with a negative value of the separation ratio.

2 The governing equations and numerical tools

We consider Boussinesq binary-fluid convection in a narrow annular cell in the presence of a vertical gravitational field $\mathbf{g} = -g\hat{\mathbf{e}}_z$. A vertical temperature gradient is imposed by fixing a temperature difference ΔT between the horizontal plates, with the temperature at the bottom being higher than at the top. We are interested in modelling experiments in cells with cross section width of the same order of the height d and mean circumference L much larger than d. In such systems convection settles in the form of straight rolls with the axis in the radial direction, the dynamics being purely 2D. Ignoring variations along the roll axes, we use a simplified

geometry consisting of a two dimensional domain $(x, z) \in [0, L] \times [0, d]$, with the aspect ratio Γ defined as $\Gamma = L/d$ much greater than one. The use of Cartesian coordinates is justified due to the small curvature of the cells used in experiments. This system admits the following basic conductive state with constant gradients of temperature and concentration

$$\mathbf{u}_c = 0, \tag{1}$$

$$T_c = T_0 - \Delta T \left(\frac{z}{d} - \frac{1}{2} \right), \tag{2}$$

$$C_c = C_0 + C_0(1 - C_0) S_T \Delta T \left(\frac{z}{d} - \frac{1}{2} \right), \tag{3}$$

where $\mathbf{u} = (u, w)$ is the velocity field; T and C are the fields of temperature and concentration of the denser component, respectively; T_0 and C_0 are their mean values, and S_T is the Soret coefficient.

The dynamics of the system is governed by the continuity equation, the Navier–Stokes equations and the energy and mass conservation equations. In their nondimensional form, scaling length with the height of the layer d, time with the vertical thermal diffusion time d^2/κ, κ being the thermal diffusivity, and temperature with ΔT, the equations explicitly read

$$\nabla \cdot \mathbf{u} = 0, \tag{4}$$

$$\partial_t \mathbf{u} + (\mathbf{u} \cdot \nabla)\mathbf{u} = -\nabla p + \sigma \nabla^2 \mathbf{u} + R\sigma[(1 + S)\Theta + S\eta]\hat{\mathbf{e}}_z, \tag{5}$$

$$\partial_t \Theta + (\mathbf{u} \cdot \nabla)\Theta = w + \nabla^2 \Theta, \tag{6}$$

$$\partial_t \eta + (\mathbf{u} \cdot \nabla)\eta = -\nabla^2 \Theta + \nabla^2 \eta. \tag{7}$$

Here, Θ denotes the departure of the temperature from its conduction profile, $\Theta = (T - T_c)/\Delta T$, and $\eta = -(C - C_c)/(C_0(1 - C_0)S_T \Delta T) - \Theta$. The dimensionless parameters in the above equations are the Rayleigh number R, the Prandtl number σ, the Lewis number τ and the separation ratio S, defined as

$$R = \frac{\alpha \Delta T g d^3}{\kappa \nu}, \qquad \sigma = \frac{\nu}{\kappa}, \qquad \tau = \frac{D}{\kappa}, \qquad S = C_0(1 - C_0)\frac{\beta}{\alpha} S_T,$$

where α and β are the thermal and concentration expansion coefficients, ν is the kinematic viscosity and D is the mass diffusivity.

The boundary conditions are taken to be periodic in x with period Γ. No-slip, fixed temperature and no mass flux at the top and bottom plates are considered

$$\mathbf{u} = \Theta = \partial_z \eta = 0 \qquad \text{on } \; z = 0, \; 1. \tag{8}$$

As a measure of the heat transport by convection, we use the Nusselt number Nu, defined as the ratio of heat flux through the top plate to that of the corresponding conductive solution. It has the following expression

$$Nu = 1 - \Gamma^{-1} \int_{x=0}^{x=\Gamma} \partial_z \Theta(z = 1) \, \mathrm{d}x.$$

We will also evaluate, as an estimate of the strength of the convection, the dimensionless quantity E_k, defined by

$$E_k = \Gamma^{-1} \int_{x=0}^{x=\Gamma} \int_{z=0}^{z=1} \mathbf{u} \cdot \mathbf{u} \, \mathrm{d}x \, \mathrm{d}z,$$

which is directly related to the mean kinetic energy of the system.

To integrate the equations in time, we have used the second order time-splitting algorithm proposed in [32], combined with a pseudo-spectral discretization in space (Galerkin–Fourier in x and Chebyshev–collocation in z). The Helmholtz and the Poisson equations resulting from

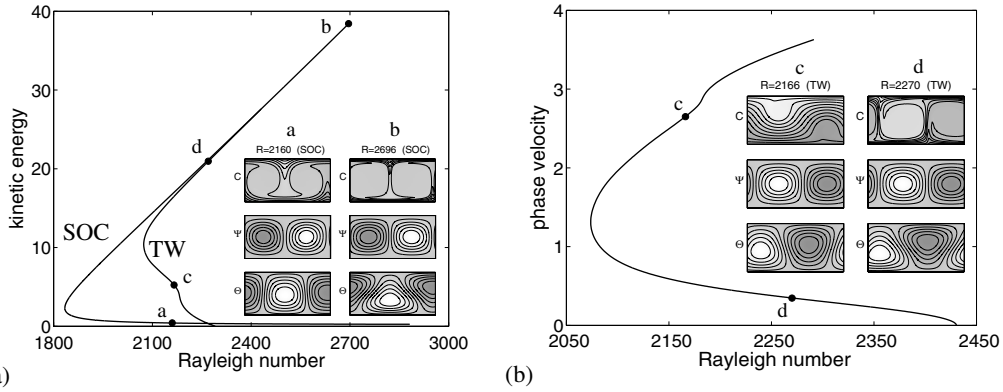

Fig. 1. $S = -0.257$, $\sigma = 9.16$, $\tau = 0.008$ (a) Bifurcation diagram showing the kinetic energy as a function of the Rayleigh number for the TW and stationary branches of spatially periodic solutions with wavenumber $k = \pi$. The contour plots correspond to concentration, streamfunction and temperature fields of a stationary state for two different values of the Rayleigh number ($R = 2160$ and $R = 2696$). (b) Phase velocity of the solution in the TW branch, and contour plots of the same fields for two TWs computed in the lower part ($R = 2166$) and in the upper part ($R = 2270$) of the TW branch of figure 1(a).

the time-splitting are solved by using a diagonalization technique [33]. In addition, to calculate the steady solutions and the spatially uniform travelling waves, both stable and unstable, in an efficient way we have adapted a pseudo-spectral first-order time-stepping formulation to apply Newton's method [34,35]. We are also able to carry out an Eckhaus stability analysis of these solutions using Floquet theory, as we presented in [30]. Finally, we have performed a 3D linear stability analysis of the conduction state, the details of the computation can be found in [31], and we have generalized the 2D time evolution code to 3D, considering adiabatic boundary conditions for temperature in the transverse direction y and applying a Chebyshev–collocation discretization in y.

In all our simulations we have used 32 collocation points in the vertical direction z, and 1200 points in the horizontal direction x to ensure sufficient resolution of the boundary layers of the concentration field. A time step of 10^{-3} has proved to be sufficient to achieve convergence. Computations with a larger resolution (32×2000) and smaller time-step ($5 \cdot 10^{-4}$) have been carried out regularly to ensure that no significant changes were observed in the solutions.

3 TW and SOC states

In large aspect ratio annular containers, spatially uniform solutions in the form of stationary and travelling wave convective rolls (TW and SOC states) can be selected by the system. These solutions consist of pairs of rolls with their axis oriented radially. The number of pairs of rolls of the structure gets adapted to the size of the container. The bifurcation diagram in figure 1(a), where the kinetic energy of the solution has been plotted as a function of the Rayleigh number, shows the branches of spatially uniform TW and SOC solutions for a $S = -0.257$ mixture computed with wavenumber $k = \pi$, which is the critical wavenumber in the cells of aspect ratio $\Gamma = 60, 80, 84$ that we have simulated. Considering $k = \pi$ in a $\Gamma = 80$ cell corresponds to a solution formed by $n = 40$ pairs of convective rolls.

For sufficiently negative values of the separation ratio, the primary instability of the conduction state is oscillatory. This instability gives rise to a branch of travelling waves that bifurcates subcritically from the conduction state for $R_c = 2291.4$. These TWs, which can either travel to the right or to the left, are unstable at the onset of convection and typically acquire stability in a secondary saddle-node bifurcation located at $R_{sn}^{tw} = 2073.7$. When the Rayleigh number is increased from the saddle-node point, the TW branch disappears for $R^* = 2431$ in a parity-breaking bifurcation of steady solutions (SOC solutions), to which stability is transferred. The

phase velocity of the TWs has been represented in figure 1(b), and as can be appreciated in the plot it decreases monotonically from its Hopf value at the onset of convection R_c to zero at the bifurcation point that gives rise to the stable stationary states R^*. As far as the branch of SOC states is concerned, it emerges from $+\infty$ in the case of a periodic cell, so it is not connected with the conductive state. The SOC branch contains also a saddle-node bifurcation point, which in this case is located at $R^s_{sn} = 1834.3$.

The contour plots of concentration, streamfunction and temperature fields for two SOC solutions computed in two different locations of the branch have been included in figure 1(a), while those corresponding to two different TWs have been plotted in figure 1(b). An outstanding feature of these fields is the strongly nonharmonic trapezoidal form exhibited by the concentration field for solutions in the upper part of the branch, both for TW and stationary solutions. While temperature and velocity fields are nearly harmonic, concentration develops narrow boundary layers, which separate regions of nearly uniform concentration (equal in the case of the SOC solution and different in the TWs). The concentration plumes become narrower and steeper as the Rayleigh number increases. The structure of the TW and SOC states has been discussed extensively in the work of Lücke et al. [26].

The bifurcation diagram shown in figure 1, as well as most of the available numerical simulations on binary convection, has been obtained in the 2D approximation, that is, the spanwise direction is not included in the computations. In terms of the transverse width of the convective rolls, the 2D approximation assumes infinite width. Nevertheless, experiments are usually performed on narrow cells in order to suppress 3D instabilities (i.e. transverse aspect ratio cells of 1.28 and 1.63 are used in [5,11]), so the 2D approximation may not seem to be justified beforehand. Alternatively, other computations reproduce convection in very narrow cells (Hele-Shaw

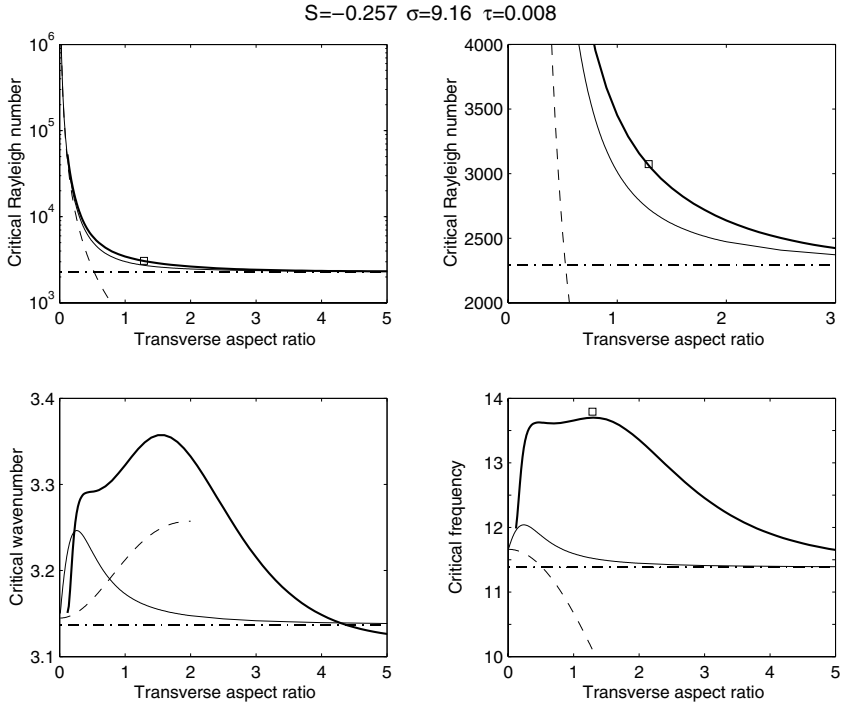

Fig. 2. $S = -0.257$, $\sigma = 9.16$, $\tau = 0.008$. Comparison of the neutral stability curves (critical Rayleigh number, frequency, and wavenumber as a function of the transverse aspect ratio, which is the ratio of the transverse width of the cell to its height) obtained by solving the 3D stability problem (thick solid line), and by using the non-ideal Hele-Shaw (thin solid line) and the Hele-Shaw (dashed line) approximations. The dashed-doted lines show the critical values resulting from the 2D approximation (bulk mixture), and the squares show the critical values found in the experiment reported in [5].

cells, where a parabolic profile for the velocity is assumed) or include approximations such as the non-ideal Hele-Shaw approximation [36], which try to model the presence of the transverse walls in intermediate-width cells.

To quantify the effect of the transverse walls on the onset of convection, we performed the linear stability analysis of the basic conductive state for a binary mixture in a narrow three-dimensional (3D) periodic cell [31], and compared the results with those obtained with the Hele-Shaw and the non-ideal Hele-Shaw approximation. Figure 2 summarizes the main results we obtained. The first conclusion that can be inferred from the plot is that the Hele-Shaw approximation cannot be used to model intermediate aspect ratio cells such as those considered in the experiments we are interested in, since the critical values resulting from this approximation are only correct for extremely narrow cells. As for the curves corresponding to the non-ideal Hele-Shaw approximation and to the 3D computations, although they reproduce correctly the Hele-Shaw limit (very narrow cells) and the bulk mixture limit (infinite aspect ratio cells), they differ for a wide range of intermediate aspect ratio values. The friction of the transverse walls on the fluid results in an increase of the critical Rayleigh number, but our results show that the non-ideal Hele-Shaw approximation underestimates this effect. It is worth noticing also that the differences between the 3D and the 2D computations extend for a much wider range of aspect ratio values than would be expected from the non-ideal Hele-Shaw results. Finally, the comparison with the experimental values reported in [5] (a square in the plots) gives an excellent agreement in the critical values between the 3D computations and the experiment. The numerical values obtained in the different cases are included in table 1.

Table 1. Experimental [5] and numerically computed values of the critical parameters for a binary mixture with $S = -0.257$ contained in a cell of transverse aspect ratio $\Gamma_y = 1.288$.

	R_c	k_c	ω_c
Experiment	3074 ± 17	3.278	13.8
3D computation	3063	3.35	13.7
Non-ideal Hele-Shaw	2726	3.16	11.5
2D computation	2292	3.137	11.4

Therefore, 3D simulations would be required to exactly match the location of the different bifurcations presented in figure 1 to experimental measurements. This notwithstanding, the essential features of the dynamics reported in experiments are definitely reproduced with the 2D simulations, and practically all the regimes reported in experiments have been obtained without the need of 3D computations. To illustrate this fact, in figure 3 we show a SOC state obtained in a cell of transverse aspect ratio 1.288 with a 3D time evolution code. Surfaces of constant concentration and temperature are depicted. The concentration plumes are clearly appreciated in figure 3(a), and we can appreciate that variations along the transverse direction are small, so the structure remains essentially 2D.

4 The role of the Eckhaus–Benjamin–Feir instability in the TW branch

A fundamental question in pattern selection and dynamics in nonequilibrium systems involves understanding the mechanism by which a periodic pattern changes wavelength in response to changes in a control parameter. This can occur through the growth of long-wavelength phase modulations, conventionally referred to as the Eckhaus instability or Eckhaus–Benjamin–Feir instability in the case of travelling waves.

In periodic extended systems, solutions with slightly different wavelengths can fit into the domain, and multistability and transitions between these states is expected to occur. In this section, we analyze the stability of spatially uniform travelling waves of different wavenumber with respect to perturbations that modify the periodicity of the basic solution, that is, we

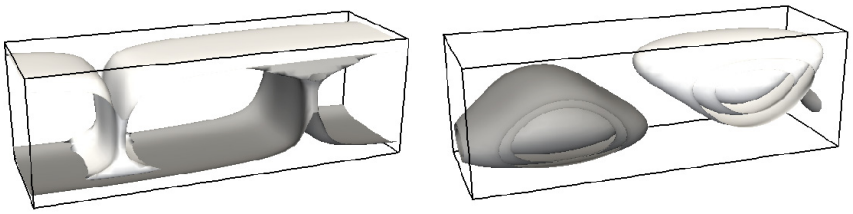

Fig. 3. $S = -0.257$, $\sigma = 9.16$, $\tau = 0.008$, $k = \pi$, $\Gamma_y = 1.288$. Surfaces of constant (left) concentration and (right) temperature perturbation corresponding to a stable three-dimensional SOC state.

compute the Eckhaus–Benjamin–Feir instability in the TW branch. Additionally, we study the dynamics triggered by this instability. We consider the particular case of the mixture used in the experiment of Baxter et al. [9], with parameters $S = -0.127$, $\sigma = 6.86$ and $\tau = 0.0083$. The experiment was performed on an annular cell of aspect ratio $\Gamma = 84$.

In annular containers the basic wavenumber of the arising pattern k is a discrete quantity, since the number of pairs of rolls of the solution gets adapted to the size of the cell. The critical wavenumber for a $\Gamma = 84$ cell is $k = \pi$, which corresponds to a travelling wave of wavelength $a = 2$ consisting of $n = 42$ pairs of rolls. In large aspect ratio annular cells, stable uniform travelling waves with a slightly different value of the wavenumber can coexist with the critical solution. These solutions, which represent travelling waves with a different number of roll pairs, i.e. $n = \ldots 40, 41, 43, 44 \ldots$ in a $\Gamma = 84$ cell, bifurcate from the conduction state for a value of the Rayleigh number very close to the critical one. Therefore, it is of interest to analyze not only the TW with wavenumber $k = \pi$, but also its neighbouring solutions.

To begin, we consider uniform travelling waves with basic wavenumber $k = \pi$ ($n = 42$ pairs of rolls). The bifurcation diagram of this solution is analogous to that shown in figure 1 for a $S = -0.257$ mixture. In order to find out whether this diagram is modified or not when the periodicity of the basic solution is allowed to change, we have computed the Eckhaus–Benjamin–Feir instability in the TW branch, both in the lower part of the branch, before the saddle-node bifurcation point, where travelling waves are unstable, and in the upper part, after the saddle-node point. Our computations show that, although several subharmonic bifurcations in the lower part of the TW branch have been identified, the stability of the $k = \pi$ TW branch is only very slightly modified when the Eckhaus instability is taken into account. Starting at the onset of convection and with very small amplitude, if the Rayleigh number is slightly decreased to follow the TW branch, the first destabilizing Eckhaus bifurcation in the TW branch has a Floquet parameter $d_1 = 1/42$ (see [30] for a definition of Floquet parameter) and takes place very close to the onset of convection. Successive destabilization against perturbations of different Floquet parameter occur, but the TW solution regains stability against most of these perturbations before the saddle-node point is reached. The last stabilizing Eckhaus bifurcation takes place in the upper part of the branch for a Rayleigh number $R = 1864.26$, which is slightly superior to that of the saddle-node, $R_{SN}^{TW} = 1863.66$. No more Eckhaus bifurcations have been identified in the upper part of the TW branch, so the travelling waves remain stable until their connection with the SOC branch.

For solutions with different wavenumber, the region of stability of the uniform TW depends very much on whether the number of rolls is increased or decreased with respect to the critical number of rolls. For the $n = 43$ TW, the last Eckhaus bifurcation that stabilizes the TW takes place at a Rayleigh number greater than the one corresponding to the saddle-node point, but the solution goes on being Eckhaus stable in a significant region. When there is a decrease in one roll pair, $n = 41$ TW, the last Eckhaus bifurcation is shifted upwards in the branch. As a result, the $n = 41$ TW is stable in a considerably smaller region than the $n = 42$ and $n = 43$ TW. This result seems to indicate that there is a trend to favour the stability of solutions with wavenumber larger than the critical one (solutions with a larger number of roll pairs).

The Eckhaus instability band can be clearly visualized in figure 4. In this figure we plot the Rayleigh number at the onset of convection (squares), the Rayleigh number at which the

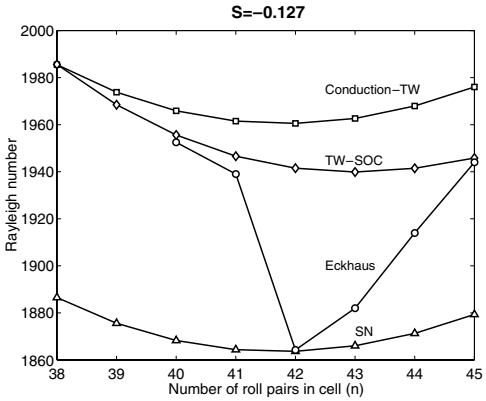

Fig. 4. Stability boundaries in a wavenumber (n)-Rayleigh number diagram corresponding to solutions for the parameters $S = -0.127$, $\sigma = 6.86$, $\tau = 0.0083$, $\Gamma = 84$. The bifurcation points for travelling waves containing different number n of roll pairs are indicated by using: squares for the bifurcation of the conductive state, triangles for the saddle-node bifurcation of TW solutions, diamonds for the parity breaking TW-SOC bifurcation and circles for the Eckhaus bifurcation which stabilizes the TW branch.

TW-SOC transition takes place (diamonds), the position of the last stabilizing Eckhaus bifurcation (circles) and the saddle-node point in the TW branch (triangles) as a function of the number of roll pairs in the cell. This defines the four corresponding stability curves. As can be inferred from the plot, travelling wave solutions containing $n = 38$, $n = 39$ or $n = 46$ pairs of rolls, are always unstable. As a consequence, for these cases the SOC solution is also unstable after the TW-SOC bifurcation. The Eckhaus bifurcation that stabilizes the solutions with these wavenumbers now takes place in the SOC branch.

Once the Eckhaus boundaries are determined it is of interest to analyze the features of the dynamics that this instability triggers. To do this, we run the time evolution code for a Rayleigh number outside the stability band, giving as an initial solution uniform TW states with different number of roll pairs.

If the number of rolls of the solution is higher than the critical value $n = 42$, two different behaviours are observed. For the $n = 43$ TW, the system makes a transition back to the conductive state for all the trials we have made with several values of the Rayleigh number. During the transient, the dominant mode decreases in amplitude and the rest of modes begin to grow, as if a phase slip leading to a change in the wavenumber was going to take place, but finally the system is unable to select a stable state different from the conductive one. In the case of the $n = 44$ TW, when the Eckhaus stability limit is approached from the stable side, a transition to a $n = 42$ TW state takes place (see figure 5). The phase modulations induced by the Eckhaus instability, which travel in the same sense as the TW and are highly localized, result in the successive annihilation of two pairs of rolls. In this case, the relaxation back to the stable wavenumber band is relatively simple, and few different states are approached by the system during the transient.

If the number of rolls of the TW is decreased in a unity with respect to the critical state, the uniform $n = 41$ TW undergoes a longer transition (see figure 6), which ends up again in a $n = 42$ TW state. In this case, as can be appreciated in the space-time plot in figure 6, while the TW travels to the right, the group velocity of the phase modulations has the opposite sense. Besides, the wavenumber modulation affects a wider region of the cell than in the previous case (transition of the $n = 44$ TW to the $n = 42$ TW). We do not observe the tendency of the system to execute damped oscillations in mean wavenumber before settling down to a stable state inside the Eckhaus band that is reported in experiment [8].

Therefore, our numerical results agree with the experimental observations about the nature of the Eckhaus instability [8,9], which is subcritical and consists of phase modulations that

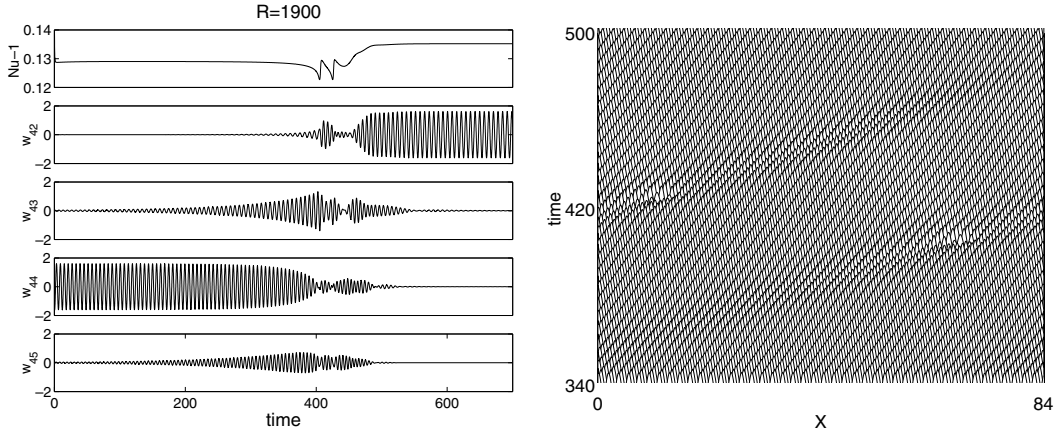

Fig. 5. $S = -0.127, \sigma = 6.86, \tau = 0.0083, \Gamma = 84$ (Left) Temporal series showing the variation of the Nusselt number and of the $n = 42$, $n = 43$, $n = 44$ and $n = 45$ horizontal mode of the vertical velocity and (right) space-time plot of the temperature during a transient that brings the solution back inside the Eckhaus instability band. The initial solution is a $n = 44$ TW state, which is Eckhaus unstable for the Rayleigh number we consider, $R = 1900$. The $d = 1/44$ Eckhaus instability triggers at first order the growth of the $n = 43$ and $n = 45$ adjacent modes. However, the system finally selects the $n = 42$ TW state that appears as a result of higher order non-linear interactions, rather than the $n = 43$ TW state, which is also Eckhaus stable for $R = 1900$.

trigger the creation or annihilation of roll pairs, although the transients observed in experiments are far more complex.

Finally, our results for the $n = 40$ TW do not allow us to understand completely the dynamics in the neighbourhood of the Eckhaus instability. In some runs, the $n = 40$ TW state is quenched outside the Eckhaus boundary and the long transients lead to a $n = 42$ stationary state, which is still stable for the Rayleigh we consider. This result is consistent with the Eckhaus instability being subcritical. However, near the Eckhaus bifurcation of the $n = 40$ TW, we have also obtained a branch of weakly modulated travelling waves, although its dynamical behaviour does not fit well the expected behaviour if the Eckhaus bifurcation were supercritical. Nevertheless, it is important to notice that this region of the parameter space ($R \approx 1950$) is complicated from the dynamical point of view, since the TW-SOC bifurcation point is extremely close to the Eckhaus bifurcation. The parameters we are considering are very close to a codimension-two point.

Depending on the value of the separation ratio of the mixture other behaviours can take place. In [30], the Eckhaus–Benjamin–Feir instability is computed for mixtures with $S = -0.021$ and $S = -0.257$.

5 Spatially non-uniform solutions

Apart from the spatially uniform TW and SOC solutions, either stable or unstable to Eckhaus instabilities, a variety of additional patterns, which can turn out to be quite striking on some occasions, can be selected by the system in the neighbourhood of the onset of convection. In this section, we describe and discuss the main properties of some of these patterns: the complex small-amplitude states observed during the dispersive chaotic regime, and two types of localized states, travelling and stationary localized convection.

5.1 Small-amplitude states and dispersive chaos

For slightly supercritical Rayleigh numbers, a convective regime consistent with experimental observations is identified for mixtures with a weak negative separation ratio. Depending on

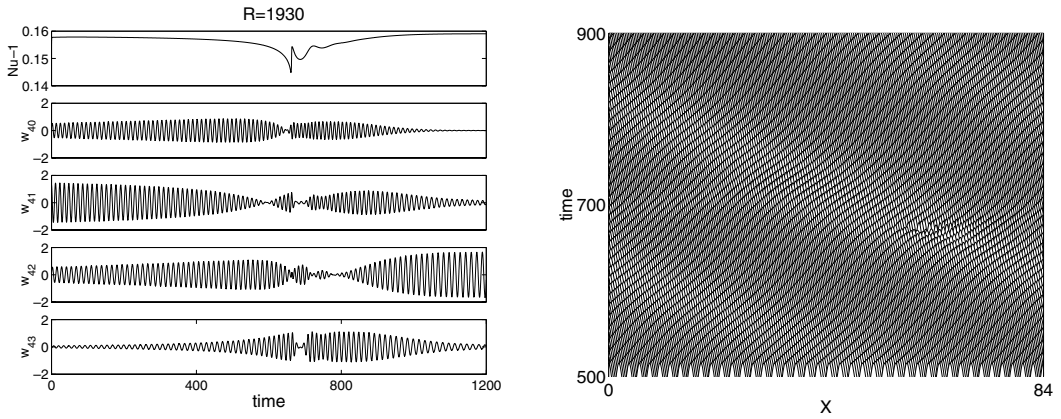

Fig. 6. $S = -0.127, \sigma = 6.86$, $\tau = 0.0083$, $\Gamma = 84$ (Left) Temporal series showing the variation of the Nusselt number and of the $n = 40$, $n = 41$, $n = 42$ and $n = 43$ horizontal mode of the vertical velocity and (right) space-time plot of the temperature during a transient that brings the solution back inside the Eckhaus instability band. The initial solution is a $n = 41$ TW state, which is Eckhaus unstable for the Rayleigh number we consider, $R = 1930$. The $d = 1/41$ Eckhaus instability triggers the growth of the $n = 40$ and $n = 42$ adjacent modes. The system finally selects the $n = 42$ TW state.

the initial conditions, the system remains in long-lived very small amplitude states instead of making a transition to the corresponding large amplitude stable state. Such small-amplitude states are never observed for subcritical values of the Rayleigh number. The dynamics we briefly discuss in this subsection has been obtained for a mixture with parameters $S = -0.021$, $\sigma = 6.22$ and $\tau = 0.009$ filling a cell of aspect ratio $\Gamma = 80$. In this case, the subcritical Hopf bifurcation of the conduction state takes place at $R_c = 1760.8$. A more detailed discussion can be found in [24].

Very close to the onset of convection ($1760.8 < R < 1765$) weakly nonlinear states of unidirectional modulated travelling waves and states of counter propagating wavepackets are observed both in experiments [23] and in simulations [24]. The first type of state consists of slightly modulated travelling waves in which the modulation travels in the same direction as the travelling wave. Although the system remains a long time in this regime, all the simulations show that the amplitude of the unidirectional modulated travelling wave finally grows superexponentially and the system undergoes a transition to the fully nonlinear stationary solution. In contrast, the system persists in the second type of state, which consists of two asymmetric wavepackets propagating in opposite directions along the cell. The stabilizing effect of the nonlinear interaction between oppositely propagating travelling waves is a well-known property that can be modelled by writing two CGL equations for the amplitudes of the right and left travelling waves [37]. Each equation contains a cubic cross term responsible for the stabilizing effect. In agreement with experimental observations, the amplitude of convection remains very small.

Remarkably, all these very small amplitude states are preceded by strong bursts of convection amplitude. The increase in the control parameter provokes the initial nearly uniform TW to grow to a large amplitude, but the mutual reinforcement of amplitude and wavenumber spatial gradients would cause the collapse of the structure. After the collapse the system ends up in a very small-amplitude state, but during the bursts of convection, the patterns clearly depart from a weakly nonlinear regime at some stages of the evolution.

A slight increase in the Rayleigh number produces a transition from the counterpropagating regime to the dispersive chaos regime. The dynamics becomes erratic and the Nusselt number oscillates aperiodically. The features of the dynamics during such regime can be appreciated in figure 7. The amplitude of convection of these states remains small until sudden bursts of convection amplitude take place in the system. This sequence of small amplitude convection followed by a burst and the subsequent collapse of amplitude repeats irregularly. The frequency

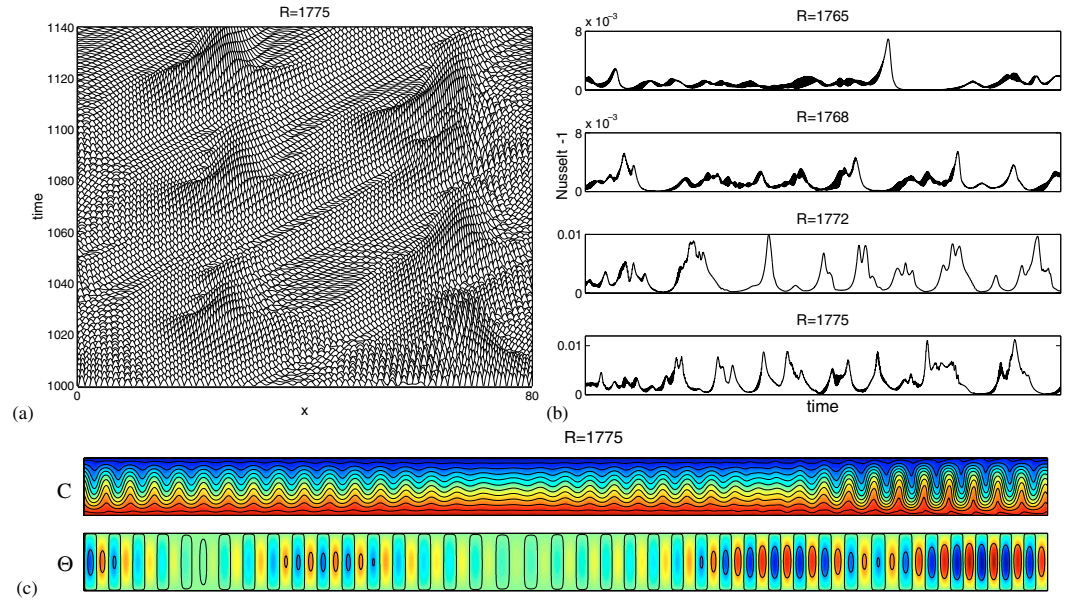

Fig. 7. $S = -0.021$, $\sigma = 6.22$, $\tau = 0.009$, $\Gamma = 80$. (a) Space-time plot of midplane temperature for a dispersive chaotic solution obtained at $R = 1775$. (b) Temporal series showing the variation of the Nusselt number for different values of the Rayleigh number during the dispersive chaotic regime. (c) Concentration and temperature contour plots of the solution for $R = 1775$ at $t = 1000$.

and intensity of these bursts changes in each episode, and these two magnitudes increase as the Rayleigh number is increased. Spatially localized travelling pulses of convection, of different length and duration, grow and decay around the cell. As the Rayleigh number increases, the variations of the structure in time are more rapid and the dynamics becomes more erratic; the pulses appear more densely in space.

The dispersive chaos regime is caused by the strong nonlinear dispersion of the system and is persistent, that is, the system can remain indefinitely in such states. Nevertheless, in some occasions our simulations show that the system makes a transition to a large-amplitude non-travelling localized state of the type described in subsection 5.3, whose length can vary. Depending on the Rayleigh number and the initial conditions, the system will follow one of several paths. Either it will remain in this localized state, or it will return to the dispersive chaos state, or it will evolve to the spatially uniform steady solution.

5.2 Localized travelling wave convection

Another interesting convective regime that can arise in a binary fluid layer heated from below close to the primary bifurcation of the conduction state is localized travelling wave convection. Such patterns consist of confined structures of travelling convection rolls that are surrounded by quiescent fluid. In annular containers, the envelope of the convectively active region drifts itself, though very slowly compared to the phase velocity of the roll pattern, while in rectangular bounded containers the envelope remains at rest, attached to an endwall. Like the extended TWs, the LTWs are observed for mixtures with a negative value of the separation ratio. The experimental, theoretical and numerical work devoted to the study of the LTWs is extensive; much attention has been paid to these structures since their first observations in rectangular cells [38,39] and in annular cells [10,11]. LTWs were obtained for the first time by direct numerical integration of the hydrodynamic field equations by Barten, Lücke et al. [6,15] in periodic containers and by Yahata [40] and Batiste et al. [41] in rectangular containers with rigid sidewalls. Here, we will briefly comment on the main features of such structures. For a

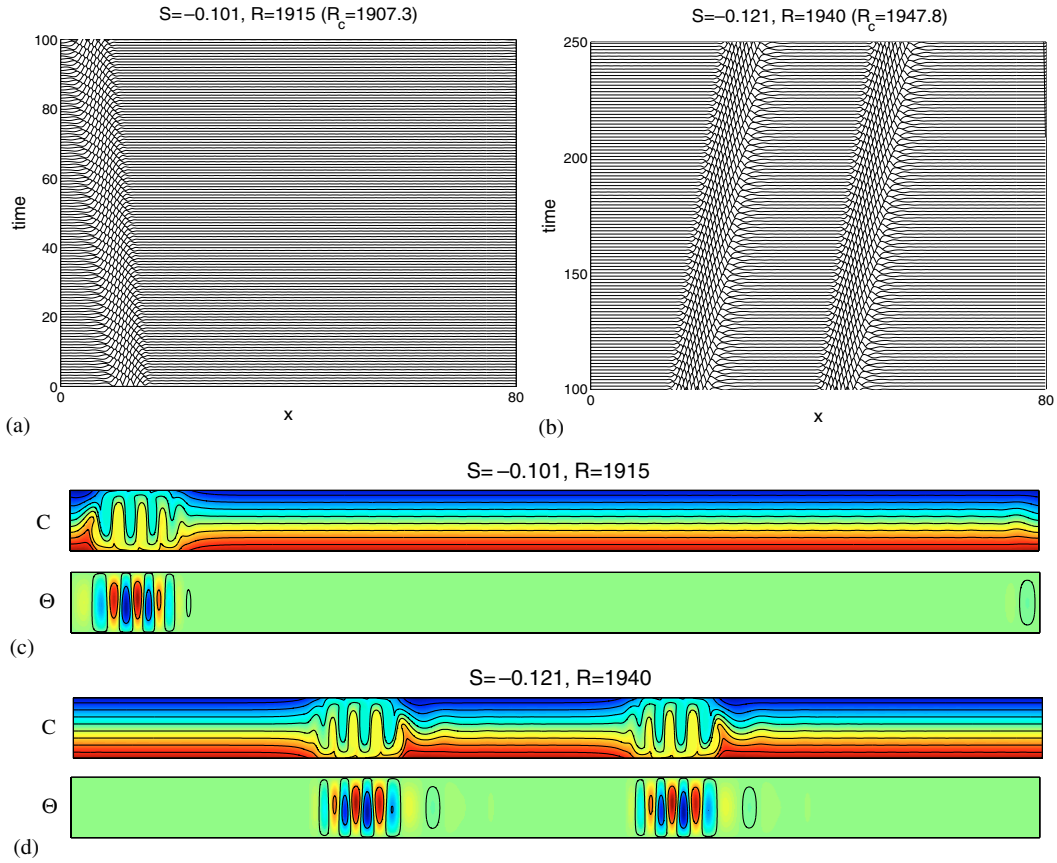

Fig. 8. $\sigma = 6.22$, $\tau = 0.009$, $\Gamma = 80$. Space-time plots of midplane temperature for (a) a localized pulse of travelling wave convection obtained for $S = -0.101$ at $R = 1915$ and (b) two localized pulses of travelling wave convection obtained for $S = -0.121$ at $R = 1940$. The corresponding temperature and concentration contour plots are depicted in (c) and (d).

complete bibliography on this subject, as well as for a nice reading on the dynamical properties of the LTWs it is worth checking [16].

To visualize the structure of a localized travelling wave, figure 8(a) shows the space-time plot of a narrow LTW obtained for a separation ratio $S = -0.101$ in a cell of aspect ratio $\Gamma = 80$. A snapshot of the contour plots of constant concentration and temperature is shown in figure 8(c). The slow drift of the LTW in the same direction as the propagation direction of the rolls inside the convective region can be clearly appreciated in the space-time plot. The magnitudes that characterize a LTW (drift velocity, oscillation frequency of the TW, length of the convective region of stable LTWs) are in general uniquely selected. The structure of a LTW is usually divided in three parts: a leading front, a central part, and a trailing front, relative to the propagation direction of the TW phase (i.e. [16]). Distinct LTWs differ only on the width of the central part; the structural properties of the fronts appear to be universal, but different for the leading and trailing fronts. In a recent work, LTWs are compared to front solutions between spatially extended TW and quiescent fluid [18].

Two types of LTWs are distinguished in literature: those observed for a weak Soret coupling (small negative value of S) and those arising in mixtures with strong Soret coupling (large negative value of S). In the first case, LTWs lie above the subcritical Hopf bifurcation at the threshold of convection $R > R_c$, and the competing extended state attractor in this case is SOC convection. In contrast, in the second case, the LTWs are subcritical with respect to R_c and they compete with extended TWs and the quiescent stable conductive state. The LTWs show richer and much more complex bifurcation behaviour in the case of stronger Soret coupling.

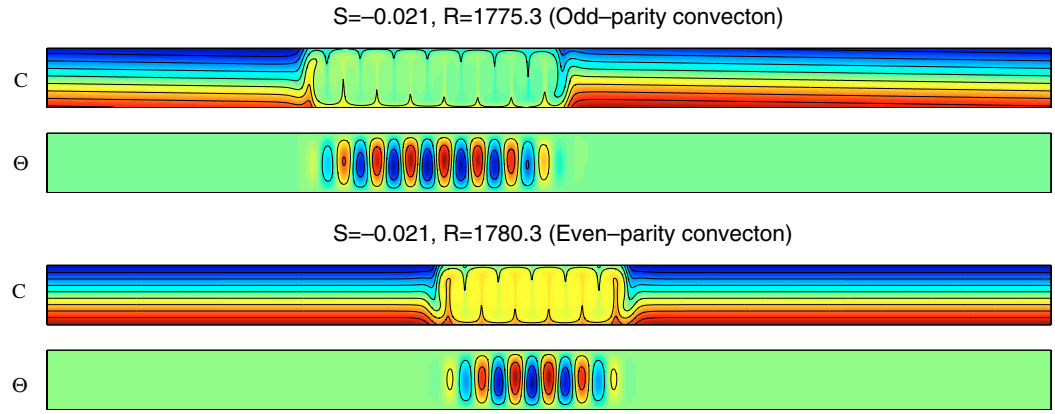

Fig. 9. $S = -0.021$, $\sigma = 6.22$, $\tau = 0.009$, $\Gamma = 60$. Concentration and temperature contour plots of an odd-parity convecton (top) and of an even-parity convecton (bottom).

The existence of stable LTWs in the case of weak Soret coupling is argued to be related with the convective unstable regime of the conductive state, since the band of existence of the LTWs seems to lie in the regime where the conductive state is convectively unstable, but not yet absolutely unstable. For $R > R_c$ the conductive state is unstable against extended TW perturbations, but localized disturbances of the conductive state can be absorbed in the LTW state, and would not have enough time to grow to an extended state.

Patterns formed by more than one LTW can also be selected by the system. In figures 8(b) and (d) the space-time plot and the contour plots of a state consisting of two localized travelling waves embedded in a region of quiescent fluid are represented. In this case, the two packets of convection are identical and travel in the same direction and at the same drift velocity. Multi-LTW states can be prepared in experiments, and are expected be stable to higher values of the Rayleigh number, since the time/space available for the disturbances to grow is reduced. The collision of LTWs has also been investigated experimentally.

5.3 Convectons

Convecton is the word coined by Blanchflower [19] to name the localized steady states present in magnetoconvection. Unlike the LTWs, convectons have not been reported in experiments on binary mixture layers. Indeed, such steady localized states have been discovered numerically, in very recent simulations of ^{3}He–^{4}He mixtures heated from below [20,21]. Subsequent simulations have confirmed their existence in water-ethanol mixtures [22], a much more experimentally accessible type of mixture. The only experimental reference to a non-travelling localized structure in binary convection is found in [23], where a water-ethanol mixture was used, though in that case the convective region was sustained by waves, instead of being surrounded by the conduction state. Convectons have also been obtained numerically in the Swift-Hohenberg equation, and their properties have been analyzed in detail in this context [42].

The structure of a convecton can be visualized in figure 9. A large amplitude region of stationary convection separated by two 'front'-like structures is embedded in the conduction regime. Inside the convection region the amplitude and wavelength of the rolls is uniform and, unlike in the localized travelling waves, concentration is nearly uniform in adjacent rolls except in the steep concentration boundary layers between rolls. The structure is completely stationary, that is, neither the convective region drifts nor the rolls travel inside it. Convectons are found below the onset of absolute instability.

A striking feature of the convectons is the arbitrariness of their length. For a fixed value of the Rayleigh number there is multiplicity of stable localized states, each formed by a different number of convection rolls. Also, two types of convectons have been obtained in simulations: odd- and even-parity convectons (see figure 9). To understand these numerical observations,

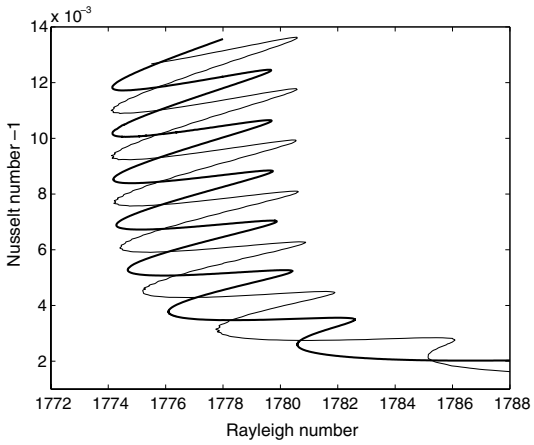

Fig. 10. $S = -0.021, \sigma = 6.22, \tau = 0.009, \Gamma = 60$. Snaking branches of odd- and even-parity convectons (thick and thin solid lines, respectively).

since convectons are stationary structures, we followed the branches of solutions using continuation techniques [22]. In figure 10 we depict the two branches of odd- and even-parity convectons that we obtained for a mixture with weak Soret coupling $S = -0.021$ in a cell of aspect ratio $\Gamma = 60$. Both the odd- and even-parity convectons lie on connected curves that 'snake' from small amplitude towards the amplitude of the coexisting extended SOC state. Stable convectons are found on portions of each branch between a left turning point and the next right turning point going up the snake. These turning points correspond to saddle-node bifurcations and, between them, as one proceeds up each snake, each convecton acquires a pair of rolls. As a result the convectons higher up each snake become broader and broader. Away from the ends of the snaking branches, the saddle-node points in each snake are lined up at the same positions (same values of the Rayleigh number), producing a well-defined pinning region in between.

In odd-parity convectons the rolls at the end rotate in the same sense, resulting in the entrainment of higher concentration at one end and lower concentration at the other end. The net effect is that the homogenized concentration inside the convecton corresponds to the average concentration. Thus, odd-parity convectons pump concentration horizontally. In contrast, rolls at the end of even-convectons rotating clockwise entrain higher concentration fluid into the convecton, while counter-clockwise rotating rolls entrain lower concentration. As a result, the mean concentration inside even-convectons can depart from its mean value.

6 Summary

In this paper we have reviewed the rich dynamics observed in binary fluid convection for mixtures with a negative value of the separation ratio. We have focused on modelling large aspect ratio annular cells for values of the parameters relevant to experiments. To do this, we have developed several accurate numerical codes based on spectral methods that enable us to compute the nonlinear states with high resolution. In general, our numerical results compare very well with experimental observations, and the possibility of obtaining numerically unstable as well as stable solutions has helped us to understand the complex dynamics found in experimental works.

Most of the spatio-temporal dynamics discussed in this paper brings together results analyzed previously in different works, but some new results are also presented. On one hand, we briefly summarize the main features of extended TWs, SOC states, and localized travelling waves. The properties of these structures have been studied in an extensive work by M. Lücke and collaborators, who provided one of the first numerical simulations of the full hydrodynamic equations. On the other, we discuss our most outstanding recent contributions, which focus on the study of structures that can only arise in extended systems. In this sense, we consider the Eckhaus–Benjamin–Feir instability of the spatially uniform TW solutions [30], which is known to play an important role in the stability of the uniform patterns, and extend the results

discussed in that work to elucidate the dynamics triggered by this instability. Additionally, we describe the properties of the small-amplitude and dispersive chaotic states arising in mixtures with weak negative Soret coupling [24], and of the localized stationary states, *convectons*, which have been discovered in binary convection very recently [20–22]. We complete the work with the study of three dimensional structures [31].

The results on the Eckhaus instability that we have presented in this paper correspond to a water-ethanol binary mixture with a separation ratio $S = -0.127$ in a $\Gamma = 84$ aspect ratio cell. The minimum of the Eckhaus stability band we have obtained is slightly shifted with respect to the experimental curve reported in [9], a discrepancy probably caused by the finite width of the experimental cell. The dynamics triggered by the Eckhaus instability has also been studied for this mixture. We have not found stable modulated TW solutions emerging from this bifurcation. Instead of these solutions, long transients which bring the solution back within the stable region or to the conductive state, have been obtained. Therefore, the dynamics obtained numerically is consistent with the subcritical nature of the instability reported in experiments [9].

The complex small-amplitude sates exhibiting bursting behaviour discussed in the paper can only be obtained in binary mixtures with a weak negative value of the Soret coupling. Our results have been obtained with a mixture of separation ratio $S = -0.021$ in a cell of aspect ratio $\Gamma = 80$, and reproduce quite satisfactorily the detailed experimental observations reported in [23]. Such states consist of the repetitive, chaotic bursting and collapse of the wave amplitude. The dynamics is dominated by the nonlinear dispersion of the system, which gets stronger by reducing the value of $|S|$. Details of the transition of the dispersive chaotic regime to states of localized convection can be found in [22,24].

On this work we have also commented on the properties of convectons, perhaps the most striking patterns arising in this system. A convecton consists of stationary rolls of uniform amplitude and wavelength, except for two front-like structures at either end that separate it from the void. They are organized into a pair of branches of different parity that snake towards the spatially periodic SOC state. As this occurs the convecton add rolls becoming the region of convection broader and broader. Preliminary results that will be extended in a future work reveal that the branches of convectons end at a certain point of the lower part of the SOC branch, emerging from a steady Eckhaus bifurcation of the SOC solution. The bigger the periodicity of the cell, the nearer to the saddle-node of the SOC branch this Eckhaus bifurcation is located.

Lastly, we have analyzed the onset of convection in 3D cells and presented preliminary results of 3D simulations in order to investigate the cause of the small discrepancies between 2D simulations and experiments.

We dedicate this work to the memory of Carlos Pérez-García, our colleague and long-time friend. He was a member of the committee for the Ph.D. thesis of A. Alonso and O. Batiste, and contacts between his group in Navarra and our group in Barcelona have been frequent throughout many years. We are grateful for his always friendly collaboration.
This work was supported by DGICYT under grant FIS2006-08954 and by AGAUR under grant 2005SGR-0024. We thank Edgar Knobloch for his helpful discussions.

References

1. M.C. Cross, P.C. Hohenberg, Rev. Mod. Phys. **65**, 998 (1993)
2. B. Echebarria, D. Krmpotić, C. Pérez-García, Physica D **99**, 487 (1997)
3. I. Mercader, J. Prat, E. Knobloch, Int. J. Bif. Chaos **12**, 2501 (2002)
4. O. Batiste, A. Alonso, I. Mercader, J. Non-Equilib. Thermodyn. **29**, 359 (2004)
5. D.R. Ohlsen, S.Y. Yamamoto, C.M. Surko, P. Kolodner, Phys. Rev. Lett. **65**, 1431 (1990)
6. W. Barten, M. Lücke, M. Kamps, Phys. Rev. Lett. **66**, 2621 (1991)
7. P. Kolodner, J.A. Glazier, H. Williams, Phys. Rev. Lett. **65**, 1579 (1990)
8. P. Kolodner, Phys. Rev. A **46**, 1739 (1992)
9. G.W. Baxter, K.D. Eaton, C.M. Surko, Phys. Rev. A **46**, 1735 (1992)
10. P. Kolodner, D. Bensimon, C.M. Surko, Phys. Rev. Lett. **60**, 1723 (1988)

11. D. Bensimon, P. Kolodner, C.M. Surko, H.L. Williams, V. Croquette, J. Fluid Mech. **217**, 441 (1990)
12. P. Kolodner, Phys. Rev. A **42**, 2475 (1990)
13. J.A. Glazier, P. Kolodner, Phys. Rev. A **43**, 4269 (1991)
14. P. Kolodner, Phys. Rev. E **50**, 2731 (1994)
15. M. Lücke, W. Barten, M. Kamps, Physica D **61**, 183 (1992)
16. W. Barten, M. Lücke, M. Kamps, R. Schmitz, Phys. Rev. E **51**, 5662 (1995)
17. D. Jung, M. Lücke, Phys. Rev. Lett. **89**, 054502 (2002)
18. D. Jung, M. Lücke, Phys. Rev. E **72**, 026307 (2005)
19. S. Blanchflower, Phys. Lett. A **261**, 74 (1999)
20. O. Batiste, E. Knobloch, Phys. Fluids **17**, 064102 (2005)
21. O. Batiste, E. Knobloch, Phys. Rev. Lett. **95**, 244501 (2005)
22. O. Batiste, E. Knobloch, A. Alonso, I. Mercader, J. Fluid Mech. **560**, 149 (2006)
23. P. Kolodner, S. Slimani, N. Aubry, R. Lima, Physica D **85**, 165 (1995)
24. A. Alonso, O. Batiste, I. Mercader, Phys. Rev. E (2007) (accepted)
25. W. Barten, M. Lücke, M. Kamps, R. Schmitz, Phys. Rev. E **51**, 5636 (1995)
26. M. Lücke, W. Barten, P. Büchel, C. Fütterer, St. Hollinger, Ch. Jung, *Evolution of Structures in Dissipative Continous Systems*, edited by F.H. Busse, S.C. Müller (Springer, Berlin, 1998), p. 127
27. B. Huke, M. Lücke, P. Büchel, Ch. Jung, J. Fluid Mech. **408**, 121 (2000)
28. P. Büchel, M. Lücke, Entropie **218**, 22 (1999)
29. O. Batiste, M. Net, I. Mercader, E. Knobloch, Phys. Rev. Lett. **86**, 2309 (2001)
30. I. Mercader, A. Alonso, O. Batiste, Eur. Phys. J. E **15**, 331 (2004)
31. A. Alonso, O. Batiste, Theor. Comp. Fluid Dynamics **18**, 239 (2004)
32. G.E. Karniadakis, M. Israeli, S.A. Orszag, J. Comput. Phys. **97**, 414 (1991)
33. S. Zhao, M.J. Yedlin, J. Comput. Phys. **113**, 215 (1994)
34. C.K. Mamun, L. Tuckerman, Phys. Fluids **7**, 80 (1995)
35. I. Mercader, O. Batiste, A. Alonso, Int. J. Numer. Meth. Fluids **52**, 707 (2006)
36. W. Schöpf, J. Fluid Mech. **245**, 263 (1992)
37. M.C. Cross, Phys. Rev. A **38**, 3593 (1988)
38. E. Moses, J. Finenberg, Phys. Rev. A **35**, 2757 (1987)
39. R. Heinrichs, G. Ahlers, D.S. Canell, Phys. Rev. A **35**, 2761 (1987)
40. H. Yahata, Prog. Theor. Phys. **85**, 933 (1991)
41. O. Batiste, E. Knobloch, Phys. Fluids **17**, 064102 (2005)
42. J. Burke, E. Knobloch, Phys. Rev. E **73**, 056211 (2006)